Wind tunnel experiment on turbulent flow field around 2D street canyon with Eaves

Tsuyoshi Sato[1*], Aya Hagishima[1], Naoki Ikegaya[1], Jun Tanimoto[1]
Interdisciplinary Graduate School of Engineering Sciences, Kyushu University,
6-1, Kasuga-Kouen, Kasuga-city Fukuoka, Japan[1]*
tsuyoshi_s@kyudai.jp
dated: 15 June 2015

1. Introduction

The turbulent flow nature around buildings has attracted much interest in both urban climatology and wind engineering, and a vast number of experiments and numerical simulations have been conducted for decades. The relationship between three flow regimes and plan area ratio is one of significant phenomenological description of this research field [Oke, 1988 [1]].

Meanwhile, most of the past studies assumed real urban geometry as idealized block arrays (e.g. Coceal et al. 2006 [2], Cheng and Castro 2002 [3]), however, in general, real urban surfaces include diverse and complicated topography derived from secondary roughness such as balconies and penthouses. Therefore, it is uncertain to what extent the airflow nature of idealized block arrays can be treated as prototypes of real urban setting. Actually, a few pioneering studies have shown the significant influence of secondary roughness on the flow field. For example, the Computational Fluid Dynamics (CFD) simulation using Reynolds-Averaged Navier-Stokes (RANS) model revealed the drastic effect of a porch on temporal-averaged flow field around 2D building models (Mohamad et al. 2014 [4]). Furthermore, they indicated that the wind-induced natural ventilation rate inside a building significantly varies with the length of a porch.

Under these circumstances, the authors have performed a wind tunnel experiment to investigate how turbulent flow field in 2D street canyon is changed by flat eaves overhang a street canyon. Time-Resolved Particle Image Velocimetry (TR-PIV) was employed to capture spatial distributions of turbulent statistics as well as unsteady flow motions around the canopy.

2. Experiment

2.1 Wind tunnel and array configuration

The closed-circuit wind tunnel with the test section of height 1.0 m, width 1.5 m and length 8 m (Fig.1) was used for the measurement of two types of canopy topography. In Case A, 40 horizontally-long bars with a cross section of 25 mm × 25 mm (hereafter, H=25mm) were arranged face to face with a 75mm interval perpendicular to the mean wind direction in the test section. On the other hand, in Case B, the 29th to 36th bar from the windward was replaced with bars attached with eaves (Fig.2). The target area for the PIV measurement was 32nd street canyon in both cases, and the eaves over the target canyon were made by transparent thin glass plates of 2mm thickness while other eaves were made by plastic plate with a same thickness. The eaves were glued on the top of horizontally-long bars with rectangular cross section (25mm×23mm) ensuring the top height of the eaves was exactly 25mm. The reference wind speed U_{20H} was approximately 2.3 m/s, and the corresponding Reynolds number based on H and U_{20H} was about 4034.

2.2 PIV set up

The plant oil particles of about 1μm diameter were used as tracers for PIV. A laser light sheet with a 1.8mm thickness was formed by the optical unit contains Nd;YAG 5W CW laser (operating at 532nm), a plano-concave lens and a convex lens (focus length is -15mm and 1000mm, respectively). The laser sheet was emitted from beneath the wind tunnel floor through a thin grass plate (Fig.1), and streamwise and vertical velocity components were measured.

The images were photographed at a frequency of 1000Hz for a period of 43.6 seconds by using a CCD camera (FASTCOM SA-X, Photron) with a lens of 85mm length f/2.8 (PC Micro-Nikkor 85mm f/2.8D,Nikon). The size of measurement area was 62.5mm×62.5mm in Case A, and the entire street canyon was measured with spatial resolution of 512pixel×512pixel. For Case B, the target area was divided into three parts and measured separately since the size limitation of camera view (each area is shown in Fig.2 (b) with red, blue and brown dotted lines). The spatial resolution of the camera was 512pixe×512pixel in the measurement for above the canyon (red line), while 512pixel×256pixel for the canopy layer (blue and brown lines). In both cases, the distance between the laser sheet and the camera was about 600mm and image magnification was about 0.17mm/pixel in all the tests.

The images were post processed by the combined algorithm of recursive cross-correlation method and image-transforming method provided by analysis software Flownizer (DITECT). Interrogation window size in each step was 31pixe×31pixel, 21pixe×21pixel, and 15pixe×15pixel, respectively. The sub-pixel scale analysis was subsequently performed via the Gaussian curve fitting method. The estimated data of velocity in the regions with proper valid signal rate and correlation coefficient were used for the following analysis (Fig.2(a)(b), black dashed line).
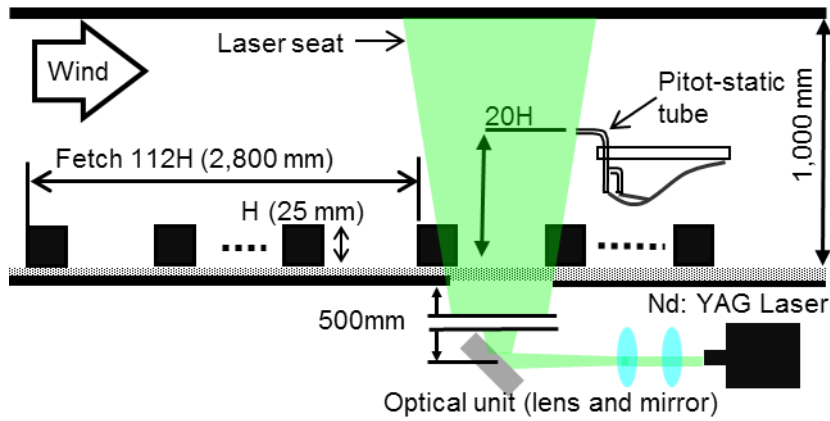
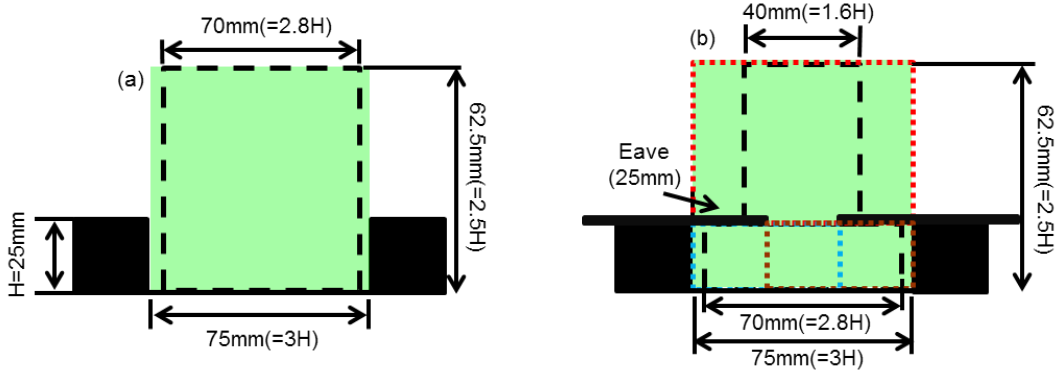Fig.1 Schematic diagram of the wind tunnel

Fig.2 Diagram of building models (a) Case A (no eaves) (b) Case B (with eaves). Dotted lines in (b): Separated measurement areas, Dashed line: the region experimental data has high accuracy

3. Result
3.1 Temporally-averaged velocity field

Fig. 3 presents temporally-averaged velocity vector maps in the two cases. In Fig.3 (a), a large recirculation eddy and a small secondary eddy behind the upstream obstacle are observed inside the canyon, and the location of centre of the primary vortex is at x/H=2.2. These characteristics correspond with the well-known features of the wake interference flow in 2D street canyon (e.g. Leonardi et al. 2003 [5]). On the other hand, in Fig.3 (b), a complicated flow structure consisting of multi-vortex arises inside the canyon. Namely, a clockwise eddy arises at the centre of the canyon, and two counter-clockwise low-speed eddies appear under the upstream and downstream eaves. Although the centre eddy is slightly larger than the other two eddies, the size of three eddies are relatively similar to each other. Although velocity is small in the large part of the canyon, the velocity at the crossover region of the centre and right eddy around x/H=2.1 is slightly large. This is probably associated with the penetration of high-speed downward flow into the canyon, and moreover, the high-speed flow is thought to be a driving force of the centre and right eddy. This supposition is consistent with features of the spatial distribution of turbulent statistics shown in the following section.
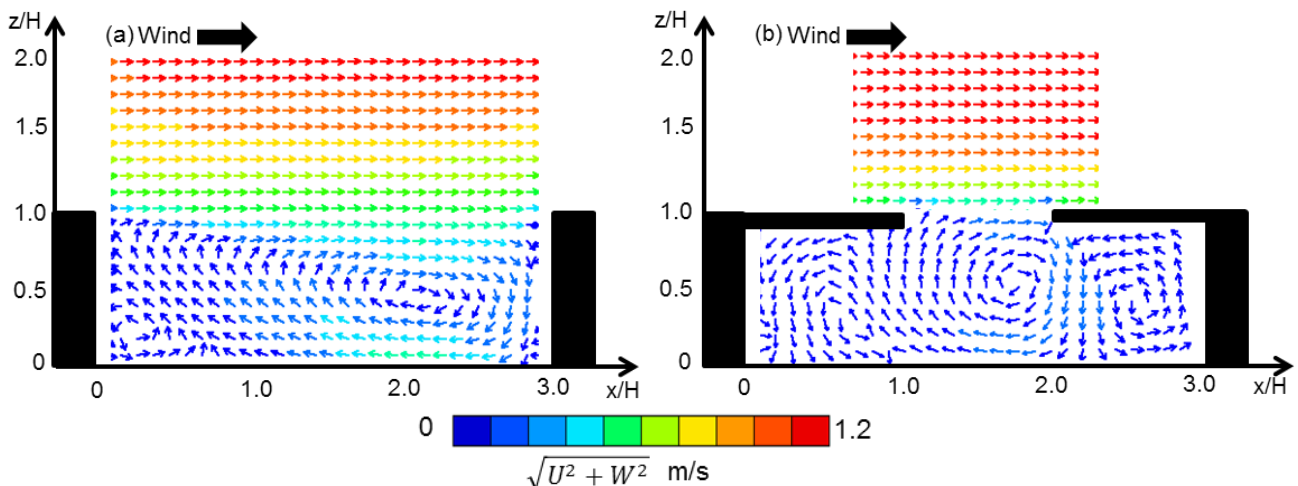

Fig.3 Temporally-averaged velocity vector maps (a) Case A (no eaves) (b) Case B (with Eaves)
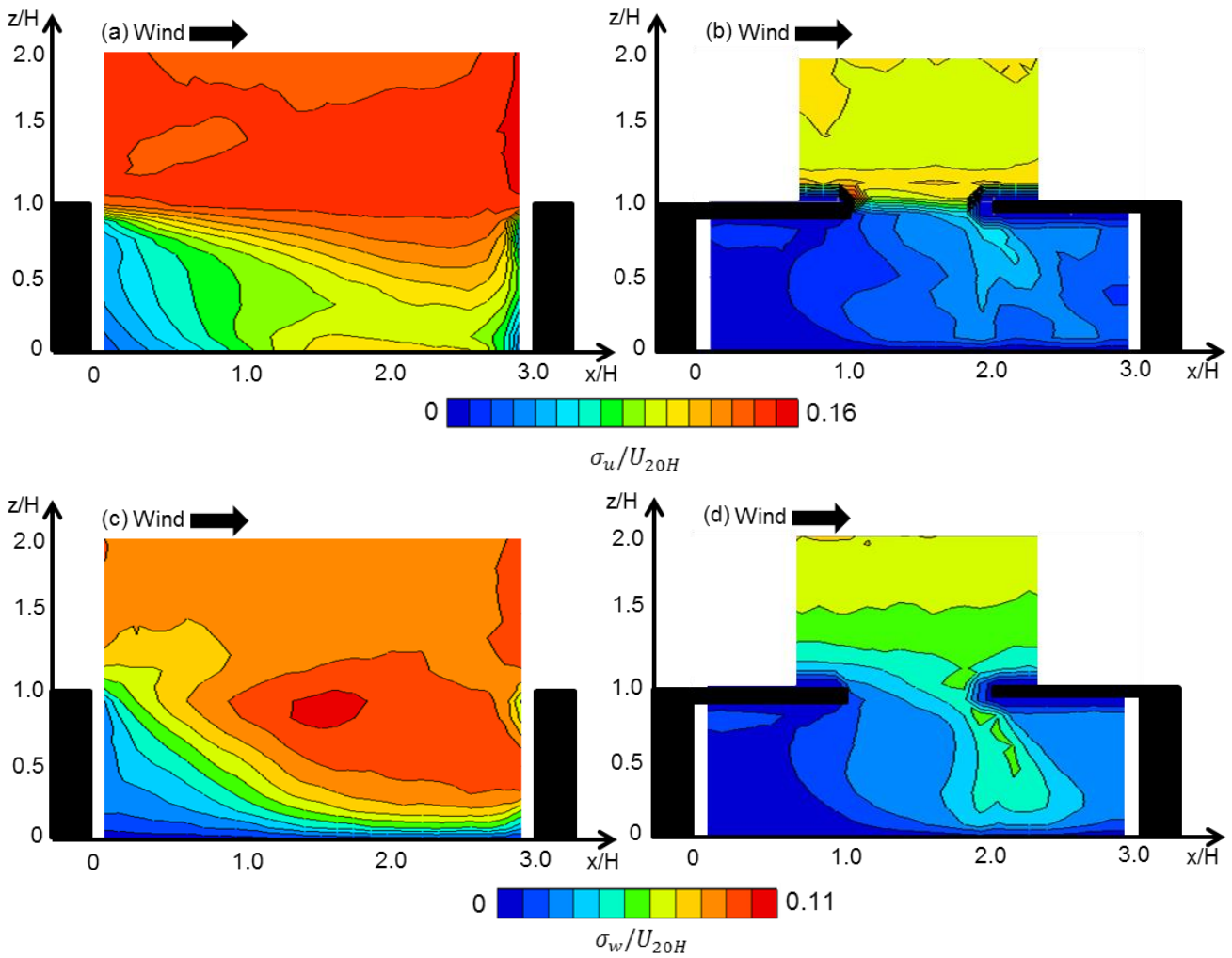
Fig.4 Spatial distributions of standard deviations. (a) and (b) are standard deviation of u normalized by reference wind speed (σ_u/U_{20H}). (c) and (d) are that of w (σ_w/U_{20H}). (a) and (c) are for Case A (no eaves) , (b) and (d) are for Case B (with eaves).
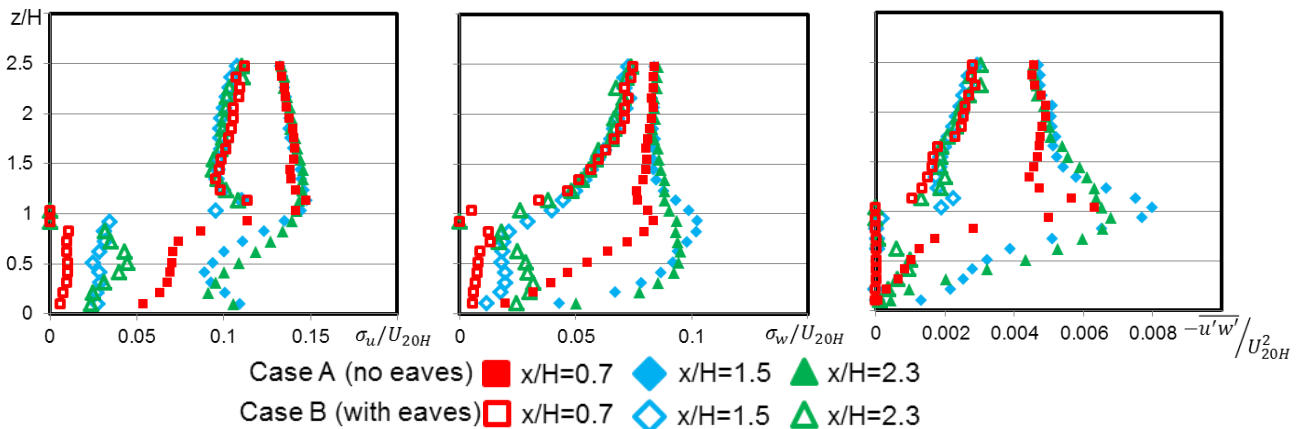

Fig.5 Profiles of turbulent statistics at three different x locations. (a)Standard deviation of u (b)Standard deviation of w (c)Reynolds stress. Values are normalized by U_{20H}.

3.2 Spacial distribution of turbulent statistics

Fig.4 presents the spatial distributions of the standard deviation of streamwise velocity normalized by the reference wind velocity (σ_u/U_{20H}), and that of vertical velocity (σ_w/U_{20H}). In addition, the vertical profiles of σ_u/U_{20H}, σ_w/U_{20H}, and $-\overline{u'w'}/U_{20H}^2$ at three different streamwise positions are shown in Fig.5.

It is obvious that the turbulent intensity becomes weak in the whole area in case B, and this fact indicates that the turbulence production by roughness is reduced by eaves. In the canyon layer, both σ_u and σ_w are almost zero at the upstream region, however, they are slightly large in a tongue-like region around x/H=2.0. This seems to be caused by the high speed flow penetrating into the canyon through the gap of eaves.

On the other hand, above the canyon, both σ_u and σ_w increase with the height in Case B contrary to Case A. This difference might not be due to the effect of eaves. In this experiment, the roughness geometry of the fetch
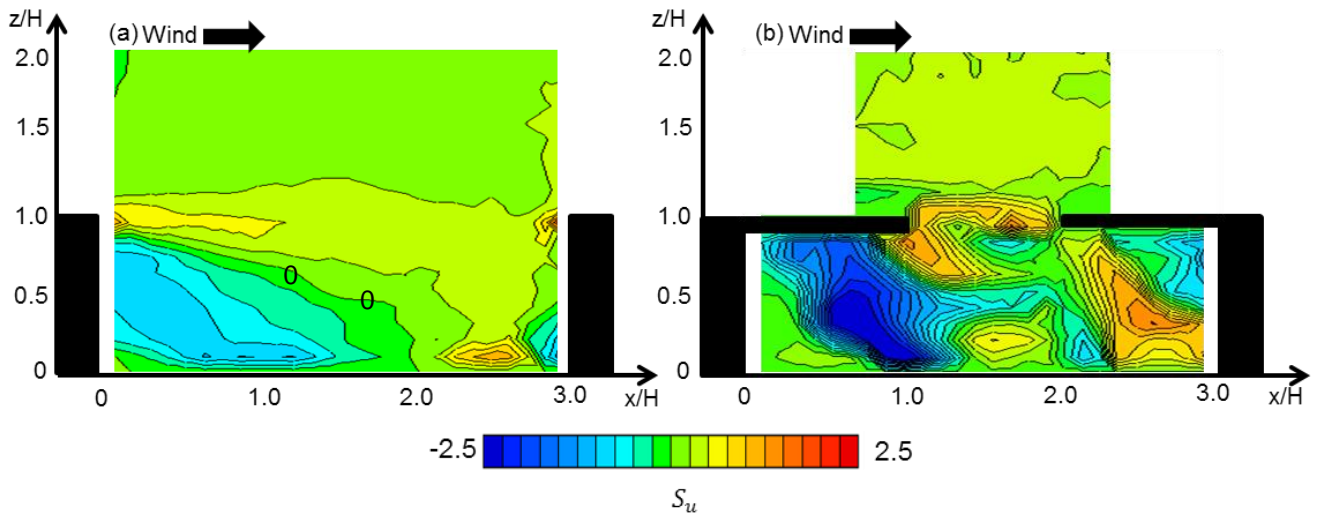
Fig.6 Spatial distribution of skewness for u. (a) Case A (no eaves), (b) Case B (with eaves)
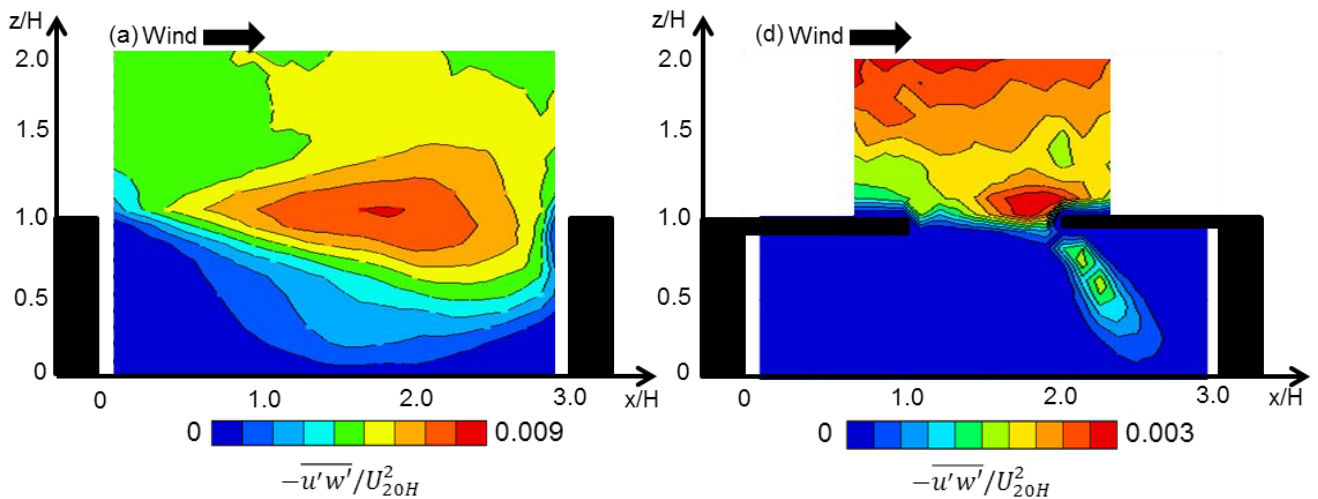

Fig.7 Spatial distribution of Reynolds stress normalized by reference wind speed ($-\overline{u'w'}/U_{20H}^2$).
(a) Case A (no eaves) (b) Case B (with eaves)

condition was fixed in both cases, and the blocks only in the area around the measured street with a streamwise length of 32H were replaced with blocks with eaves for Case B (Sect. 2.1). Thus, the internal boundary layer adjusted with the blocks with eaves was supposed not to reach to the top of photographed area. Eventually, the turbulent nature above the canopy for Case B might be affected by the boundary layer developed in the fetch section with the same geometry of Case A rather than that for the underlying blocks with eaves.

Fig.6 shows contour maps of the skewness of streamwise component (S_u). In case A, S_u is positive in the most part of the canyon, but negative behind the upstream roughness. It is noteworthy that the region of S_u <0 corresponds with the reverse flow region of the primary eddy, while the area of S_u >0 coincides with the vortex-edge where temporally-averaged u is positive.

The spatial distribution of S_u inside the canyon of Case B is much complicated compared to that of Case A, however, the relation between vortex edge and S_u is similar to the data of Case A. Namely, positive S_u arises around the upper-edge of the centre eddy and the left-edge of the right eddy, while negative S_u locates at the reverse flow region of the left eddy. Moreover, it is noteworthy that the values of S_u are almost same ($\fallingdotseq$1.5) at the opening between eaves, and the area diagonally extends between x/H=2 to 3 within the canopy. The tendencies observed in both spatial distributions of σ_u and Reynolds stress suggest that the centre and right eddy are driven by the high-speed downward flow incoming from over the canyon.

Fig.7 presents contour maps of the Reynolds stress normalized by square of reference wind velocity ($-\overline{u'w'}/U_{20H}^2$). The streamwise-elongated region of large Reynolds stress is observed at the height of 1.0H in Case A. This feature is observed in two-dimentional canyon flow regardless of the street aspect ratio (ratio of canyon width and roughness height)(e.g. Simoens et al. 2007 [6]), however, such elongated-peak of the Reynolds stress at the top of canyon does not appear in Case B although a small peak arises near the edge of the downstream eave.

4. Summary

A PIV experiment was performed to investigate how secondary roughness changes the turbulent flow nature around the roughness. The measurements reveal that the temporally-averaged flow field is drastically changed by

the eaves, causing the complicated flow field which contains multiple vortexes. According to the spatial distributions of the skewness of streamwise component, high-speed downward flow above the canyon sometimes penetrates through the gap between eaves and reaches to the bottom of the canyon, driving the two eddies in the canyon. Standard deviations and Reynolds stress are slightly large in the tongue-like regions under the downstream-side eave due to the high speed flow from above the canyon, however, the turbulent production is strongly limited by the eaves reducing turbulent intensity and Reynolds stress in the large part of the measurement area.

Acknowledgment

Reference

[1]Oke, T. R. (1988) Street Design and Urban Canopy Layer Climate. *Energy and Buildings*, 11: 103-113
[2]Coceal, O., Thomas, T. G., Castro, I. P., and Belcher, S. E. (2006) Mean Flow and Turbulence Statistics Over Groups of Urban-like Cubical Obstacles., *Boundary-Layer Meteorology,* 121, 491-519
[3]Cheng, H. and Castro, IAN P. (2002) Near wall flow over urban-like roughness, *Boundary-Layer Meteorology,* 104, 229-259
[4]Mohamad, M. F., Hagishima, A., Tanimoto, J., Ikegaya, N., and Omar, A.R. (2014) On the Effect of Various Design Factors on Wind-Induced Natural Ventilation of Residential Buildings in Malaysia. *The 2nd Asia Conference of International Building Performance Simulation Association.* Nagoya, Japan
[5]Leonardi, S., Orlandi, P., Smalley, R. J., Djenidi, L., and Antonia, R. A. (2003) Direct numerical simulations of turbulent channel flow with transverse square bars on one wall. *Journal of Fluid Mechanic*s, 491: 229-238
[6]Simoëns, S., Ayrault, M.,Wallace, J. M. (2007) The flow across a street canyon of variable width—Part 1: Kinematic description, *Atmospheric Environment,* 41, 9002-9017